Controlling septum thickness by a large protein ring

Michaela Wenzel[1,§,*], Ilkay N. Celik Gulsoy[1*], Yongqiang Gao[1¤], Joost Willemse[2], Mariska G. M. van Rosmalen[3], Gijs J. L. Wuite[3], Wouter H. Roos[4], Leendert W. Hamoen[1#]

[1]Bacterial Cell Biology, Swammerdam Institute for Life Sciences, University of Amsterdam, 1098 XH Amsterdam, The Netherlands

[2]Molecular Biotechnology, Institute of Biology, Leiden University, 2333 BE, Leiden, The Netherlands

[3]Department of Physics and Astronomy and Laser Lab, Free University of Amsterdam, 1081 HV Amsterdam, The Netherlands

[4]Molecular Biophysics, Zernike Institute, University of Groningen, 9747 AG Groningen, The Netherlands

[*]These authors contributed equally to this work.

[#]Corresponding author: Leendert Hamoen, l.w.hamoen@uva.nl

[§]Current address: Division of Chemical Biology, Department of Biology and Biological Engineering, Chalmers University of Technology, 41296 Gothenburg, Sweden

[¤]Current address: Department of Microbiology and Immunobiology, Harvard Medical School, Boston MA 02115, USA

Abstract

Gram-positive bacteria divide by forming a thick cross wall. How the thickness of this septal wall is controlled is unknown. In this type of bacteria the key cell division protein, FtsZ, is anchored to the cell membrane by SepF. We have isolated SepF homologues from different bacterial species and found that they all polymerize into large protein rings with diameters varying from 19 to 41 nm. Interestingly, these values correlated well with the thickness of their septa. By constructing different SepF chimeras, we showed that the conserved core domain of SepF determines ring diameter. Importantly, expressing SepF chimera with smaller diameters in *Bacillus subtilis* reduced septum thickness. These results support a model in which SepF polymerizes into molecular clamps on the leading edge of nascent septa, thereby controlling septal thickness. This suggests that the intrinsic shape of a protein polymer can function as a mold to shape the cell wall.

Introduction

The hallmark of Gram-positive bacteria is their thick cell wall composed of multiple layers of peptidoglycan. They divide by synthesizing a crosswall in between the newly formed daughter cells, and the thickness of this division septum approaches that of the lateral cell wall. How Gram-positive bacteria regulate the thickness of their cell wall and division septum is not known. We have investigated the latter using the Gram-positive model organism *Bacillus subtilis*.

Bacterial cell division is accomplished by a complex multi-protein machinery called the divisome. Assembly of the divisome begins with polymerization of the tubulin homologue FtsZ at midcell into a ring-like configuration, the so called Z-ring (1). This structure forms a scaffold for the late cell division proteins responsible for synthesis of the dividing septal wall (2). Several cell division proteins support the formation of the Z-ring, and a key step is the anchoring of FtsZ polymers to the cell membrane. This is achieved by the conserved peripheral membrane proteins FtsA and SepF. Both proteins directly interact with FtsZ and use an amphipathic α-helix to bind the cell membrane (6, 7). FtsA can be found in both Gram-positive and Gram-negative bacteria, whereas SepF is widely conserved in Gram-positive and Cyanobacteria, but has no known homologue in Gram-negatives (3, 4). Several bacteria, such as *B. subtilis*, contain both membrane anchors (5). Other proteins that stimulate Z-ring formation in *B. subtilis* are the conserved protein ZapA, which links FtsZ polymers (8), and the transmembrane protein EzrA that regulates FtsZ assembly (9). Once the Z-ring is assembled, the late cell division proteins arrive. These transmembrane proteins form a complex comprising the peptidoglycan glycosyltransferase FtsW (10), the transpeptidase Pbp2B (11), and the bitopic transmembrane proteins FtsL, DivIC

65 and DivIB (12). It is assumed that the latter three proteins regulate the assembly
66 of late cell division. However, for Gram-positive bacteria it is not yet clear how the
67 late proteins are recruited to the Z-ring.

68 *B. subtilis* can use either FtsA or SepF as anchor for the Z-ring, since only
69 one of them is required for Z-ring formation. However, the absence of SepF results
70 in highly deformed septa, which is not the case when FtsA is absent (4). This
71 indicates that SepF must have an additional function related to septum formation.
72 Curiously, purified *B. subtilis* SepF forms large ring structures with an inner
73 diameter of ~40 nm (5). Based on the crystal structure of SepF, these rings must
74 encompass at least 80 to 100 SepF molecules (5). *In vitro*, these protein rings are
75 able to bundle FtsZ polymers into very long microtubule-like structures with SepF
76 rings stacked perpendicularly to the FtsZ polymers (13). However, such
77 microtubular structures have never been observed in bacteria, and later studies
78 showed that the membrane-binding amphipathic α-helix of SepF is likely located
79 inside the ring, which seems to rule out ring formation *in vivo* (5). Interestingly,
80 the inner diameter of SepF rings is about the same size of the thickness of the
81 septal wall (43 nm). We wondered whether this relationship is relevant, and if so,
82 whether SepF rings might actually control the thickness of division septa. To
83 examine this, we purified SepF from different Gram-positive bacteria and found
84 that these proteins form large protein rings as well. Importantly, also in these
85 organisms there seems to be a correlation between SepF ring diameter and septum
86 thickness. As a final proof we expressed SepF chimeras with smaller diameters in
87 *B. subtilis*. Indeed, this reduced the thickness of septa. These results provide
88 strong evidence that Gram-positive bacteria regulate the thickness of their septal
89 wall by the strong curvature of SepF polymers at the leading edge of nascent septa.
90 It also indicates that the intrinsic form of a protein polymer can function as a mold

that can shape a cell wall.

92 **Results**

93

94 **SepF rings and tubules**

95 Purified *B. subtilis* SepF forms large protein rings when observed with transmission
96 electron microscopy (TEM) using negative staining with uranyl acetate (5). Since
97 high concentrations of this salt might influence the behavior of SepF and possibly
98 stimulates this ring formation, we first examined whether the protein can form
99 rings under more physiological conditions using atomic force microscopy (AFM). It
100 appeared that under these conditions purified *B. subtilis* SepF also forms rings with
101 diameters of about 40 nm (Fig. 1). Rings were 2 to 4 nm high (Fig. 1C, D), which
102 corresponds to a single or double molecule stacking, since the crystal packing has
103 shown that SepF polymers can be 1.5 or 2.6 nm wide, depending on the orientation
104 of SepF dimers (5).

105 Previously, SepF was purified as a maltose-binding protein (MBP) fusion
106 followed by proteolytic cleavage and removal of MBP using ion-exchange
107 chromatography (5, 13). We noticed that after cleavage, SepF precipitates,
108 possibly due to the presence of calcium in the digestion buffer. After resuspension
109 in calcium-free buffer, SepF formed stacks and tubules with diameters
110 corresponding to that of SepF rings when observed by TEM (Fig. 1E). After ion-
111 exchange chromatography only rings are found (Fig. 1F). These findings, together
112 with the AFM data, show that the circular polymerization of *B. subtilis* SepF is a
113 robust feature that likely also occurs *in vivo*.

114

115 **SepF from other species**

116 To determine whether ring formation is a conserved feature of SepF, we purified
117 the protein from different organisms. *Bacillus cereus* is an important food-spoiling

118 bacterium (14, 15) and the causative agent of rainforest anthrax (16–18) and was
119 chosen as close relative of *B. subtilis*. We further selected *Clostridium perfringens*,
120 *Mycobacterium tuberculosis*, and *Streptococcus pneumoniae,* all of which are
121 important human pathogens. *S. pneumoniae* differs from the rest since it forms
122 cocci instead of rods, and *M. tuberculosis* is one of the bacterial species that lack
123 an FtsA homologue. An amino acid sequence alignment of the different SepF
124 homologues is shown in Fig. 2A. The central domain of the protein, which contains
125 the FtsZ binding site (5), is particularly conserved. All proteins were successfully
126 purified as MBP fusions. *C. perfringens, M. tuberculosis,* and *S. pneumoniae* SepF
127 precipitated after proteolytic cleavage from MBP and were further purified by
128 centrifugation, whereas *B. cereus* SepF remained largely soluble and was purified
129 by ion-exchange chromatography.
130

131 **Membrane binding**

132 A key property of *B. subtilis* SepF is its capacity to bind the cell membrane, which
133 is achieved by an N-terminal amphipathic α-helix (amino acids 1-13) (5). This N-
134 terminal amphipathic helix is reasonably conserved in the different SepF variants
135 (Fig. 2A, see Fig. S1 for helical wheel depictions), although the helices differ in
136 their hydrophobicity and hydrophobic moment (Fig. S2). To confirm that the
137 different SepF molecules are able to bind to lipid membranes, the purified proteins
138 were mixed with liposomes. This caused a strong aggregation of liposomes, and
139 deformed them into small vesicles, as observed with high-resolution structured
140 illumination microscopy (SIM). One example, *S. pneumoniae* SepF, is presented in
141 Fig. 2B, C (see Fig. S3 for all variants). Such liposome deformation is a typical
142 characteristic of membrane-interacting amphipathic α-helices (19). These results
143 indicate that the membrane binding activity of SepF is conserved.

144

145 **Ring formation**

146 Another characteristic of *B. subtilis* SepF is its tendency to polymerize into a curved
147 structure. If this feature is important for the activity of SepF, it should not be
148 restricted to the *B. subtilis* protein. To check this, the purified SepF homologues
149 were spotted on TEM grids and negatively stained with uranyl acetate. Indeed, as
150 shown in Fig. 2D, all SepF variants formed large rings of a remarkably constant
151 size. However, the average ring diameters varied between species, from ~20 up
152 to ~40 nm (Fig. 2F).

153

154 **Correlation with septum thickness**

155 The different ring diameters offered a first real test of the hypothesis that SepF
156 ring diameter determines septum thickness. To this end, we performed TEM of the
157 different bacterial species and measured the diameter of nascent cell division septa
158 (Fig. 2E, G). Because of its high pathogenicity we used published data for *M.*
159 *tuberculosis* (20). As shown in Fig. 2I, there is a clear correlation between inner
160 ring diameters and the thickness of septa in the different species. Only *B. cereus*
161 did not follow this trend, with SepF rings that are clearly smaller than the width of
162 its septa (Fig. 2F-H).

163

164 **Core domain defines ring diameter**

165 Proteolytic trimming has shown that the conserved C-terminal domain of *B. subtilis*
166 SepF, spanning amino acids 57 to 151, is sufficient for the formation of rings (5).
167 Therefore, we assumed that this core domain determines ring diameter. To test
168 this, we replaced the conserved core domain of *B. subtilis* SepF with those of the
169 SepF proteins from the other species, maintaining the first 67 and last 13 amino

170 acids of *B. subtilis* SepF. These chimeras were then expressed in *E. coli*, purified,
171 and visualized by TEM using negative staining. All SepF chimeras were able to form
172 rings, and importantly, the ring diameters of these chimeras corresponded very
173 well to the diameters of the original SepF variants (Fig. 3A-D).
174
175 **Functional chimeras**
176 If it is true that the diameter of SepF rings determines the thickness of septa, then
177 expressing a SepF variant with a smaller diameter in *B. subtilis* should result in
178 thinner septa. It is unlikely that SepF from other species function in *B. subtilis*,
179 since the N- and C-termini of SepF, which are much less conserved, are crucial for
180 its activity (5, 13). Therefore, the chimeras provided a unique opportunity to test
181 this, assuming that the core domains are sufficiently conserved so that they can
182 bind *B. subtilis* FtsZ. To determine whether these chimeras are active in *B. subtilis*,
183 they were expressed in a Δ*sepF* strain. *B. subtilis* is one of the few species that
184 can grow without SepF, although this leads to strongly deformed septa (4). This
185 phenotype can be easily observed using high-resolution SIM microscopy by
186 fluorescently labelling the cell membrane (Fig. 4A). Only the *S. pneumoniae*
187 chimera failed to rescue the Δ*sepF* phenotype, while the *B. cereus, C. perfringens,*
188 and *M. tuberculosis* chimeras were all able to restore normal septum formation in
189 the Δ*sepF* background (Fig. 4A). This was also confirmed by TEM (Fig. 4B).
190 The inner ring diameter of the *C. perfringens* SepF chimera (24 nm) is
191 considerably smaller than *B. subtilis* SepF (42 nm). When this chimera was
192 expressed in the Δ*sepF* strain, the septum thickness decreased substantially from
193 43 to 28 nm (Fig. 4C, D). A similar decrease in septum thickness was observed,
194 when the *M. tuberculosis* SepF chimera (35 nm diameter) was expressed in the
195 Δ*sepF* background (Fig. 4C-E). These results strongly indicate that the SepF ring

196 diameter controls septum thickness.

197 Finally, the diameter of *B. cereus* SepF is approximately 10 nm smaller than
198 *B. subtilis* SepF (Fig. 2F), and so is the diameter of the *B. cereus* SepF chimera
199 (Fig. 3B). However, *B. cereus* has an average septum thickness comparable to that
200 of *B. subtilis* (Fig. 2G). If the core domain of SepF determines septum thickness,
201 it is likely that expression of the *B. cereus* chimera in *B. subtilis* Δ*sepF* results in
202 septa with a thickness comparable to that of wild type *B. subtilis* cells. This was
203 indeed the case (Fig. 4C-E).

204

205 **Discussion**

206

207 In this study we have shown that (i) the membrane binding and ring forming
208 activities are conserved in SepF homologues, (ii) the correlation between ring
209 diameter and septum thickness can be found in different Gram-positive bacteria,
210 and (iii) the septum thickness of *B. subtilis* cells can be reduced by expressing
211 SepF mutants with a smaller diameter. Together these findings strongly suggest
212 that the diameter of curved SepF polymers define septum thickness. The
213 positioning of SepF polymers at the division site cannot be directly observed using
214 high-resolution cryo-electron microscopy due to the electron density of the
215 bacterial cytoplasm and cell wall. However, our findings provide support for a SepF
216 clamp model (Fig. 5). Since the membrane-binding amphipathic α-helix of SepF is
217 located inside the rings, it is likely that SepF polymers do not form rings, but
218 instead form arcs, wrapping the leading edge of nascent septa, on top of which
219 FtsZ polymers bind and align. Since these arcs control the freedom of movement
220 of FtsZ polymers, including the peptidoglycan synthetic apparatus that is linked to
221 the FtsZ polymers (Fig. 5), the diameter of SepF rings will determine the thickness
222 of the septal wall. Many SepF arcs must line the leading edge of the nascent
223 septum to maintain an even thickness. This could be facilitated by the propensity
224 of SepF rings to form stacks (Fig. 1F).

225 *B. cereus* SepF behaved slightly differently and showed an average inner
226 ring diameter of 30 nm, which is smaller than its average septum thickness of 43
227 nm. Possibly, *B. cereus* SepF polymers are more flexible in a cellular environment,
228 enabling a wider diameter, or there might be other factors involved in controlling
229 septum diameter in this organism in addition to the physical confinement of SepF
230 polymers. In fact, *B. subtilis* can still make septa, albeit irregular in shape, when

231 SepF is absent, suggesting that other factors provide some control of FtsZ
232 polymers. FtsA, which also forms polymers, might be such factor.

233 Gram-negative bacteria contain a cell wall that consists of a single-layer of
234 peptidoglycan. The thickness of this layer is regulated by the outer membrane
235 proteins LpoA and LpoB, which reach through the peptidoglycan layer to contact
236 and regulate the cell membrane-anchored peptidoglycan-synthetic enzymes (21).
237 Possibly, this is why Gram-negative bacteria do not need a SepF-like protein for
238 septum thickness control. It should be mentioned that *E. coli* FtsA has been shown
239 to form ring structures *in vitro* as well (22). However, the inner diameter of these
240 rings is ~15 nm, which is considerably smaller than the width of septa.

241 Previous structural work has indicated that SepF rings are built of tightly
242 packed dimers. These dimers are formed by two parallel oriented monomers (5),
243 as a consequence all SepF dimers have the same orientation in a ring. However,
244 FtsZ polymers treadmill in both directions in the Z-ring (23), and it is likely that
245 they bind SepF rings in both polymer orientations. SepF binds to the C-terminal
246 domain of FtsZ (24), which is connected to the main protein domain by a long
247 flexible linker (25). This flexibility might enable FtsZ polymers with opposite
248 orientations to interact with the same SepF ring.

249 Regulation of the shape of septal walls by SepF through its intrinsic
250 curvature is reminiscent of the activity of MreB, which controls the rod shape of
251 many bacteria (26). MreB forms polymers of defined curvature that orientate and
252 move transversely to the long axis of cells, along the direction of greatest
253 membrane curvature (27, 28), thereby guiding the cell wall synthetic machinery
254 in a way that enforces and maintains a rod shape (29, 30). However, unlike SepF,
255 the intrinsic curvature of MreB filaments, which has been estimated to have a
256 diameter of roughly 200 nm (27), does not correlate with the diameter of the cell,

257 which is much larger (27). Thus, the control of septum thickness by a molecular
258 clamp, such as a SepF arc, is a novel concept of how protein polymers can control
259 the shape of growing cell walls.

260 **Material and Methods**

261

262 **Strain construction**

263 All strains used in this study are listed in Table S1, plasmids in Table S2, and
264 primers in Table S3. Plasmids for purification of SepF variants were constructed by
265 PCR amplification of *sepF* from the respective organisms, followed by restriction
266 cloning into the pMalC2 plasmid (31), using the *Xba*I and *Sma*I or *Eco*RI restriction
267 sites. pMalC2-based plasmids for purification of chimera proteins and pAPNC-213-
268 kan-based plasmids (32) for integration of *sepF* variants into the *aprE* locus in the
269 *B. subtilis* genome were constructed by Gibson assembly (33). pMalC2-derived
270 purification plasmids were transformed into calcium-competent *E. coli* BL21 (DE3).
271 pAPNC-213-kan-derived integration plasmids were transformed into *B. subtilis* 168
272 using a standard starvation protocol (34). Deletions of the *sepF* and *ftsA* genes
273 were introduced by transforming the resulting *B. subtilis* strains with chromosomal
274 DNA isolated from YK204 (*sepF::spc*) (35), BFA2863 (*sepF::ery*) (4), and TB94
275 (*ftsA::cat*), respectively. TB94 was created by transformation of *B. subtilis* 168
276 with chromosomal DNA of strain MD133 *ftsA::cat aprE::kan Pspac-ftsA* (35)
277 followed by selection on chloramphenicol resistance but kanamycin sensitivity.

278

279 **Protein purification**

280 *E. coli* BL21 (DE3) strains carrying pMalC2 plasmids for purification of SepF
281 variants were grown overnight in LB containing 100 µg/ml ampicillin at 37 °C under
282 continuous shaking. Cultures were diluted 1:100 and allowed to grow until an OD_{600}
283 of 0.4 in the presence of ampicillin. Expression of maltose-binding protein (MBP)-
284 tagged SepF proteins was induced by addition of 0.5 mM IPTG. Cells were
285 harvested by centrifugation after 4 h of induction and subsequently washed in

286 phosphate-buffered saline supplemented with 1 mM phenylmethylsulfonyl fluoride
287 to prevent protein degradation. Dry cell pellets were flash-frozen in liquid nitrogen
288 and stored at -80 °C until further use. Cell pellets were resuspended in buffer AF
289 (50 mM Tris-HCL, pH 7.4, 200 mM KCl, 5 mM EDTA, 0.5 mM DTT) supplemented
290 with one Complete mini protease inhibitor tablet (Roche) and disrupted by French
291 Press. Cell debris was removed by ultracentrifugation at 31,000 x g, and the
292 resulting supernatant was filtered through 0.2 µm filter membranes prior to
293 loading onto a Tricorn 10/20 column (GE Healthcare) packed with 2 ml amylose
294 resin (New England Biolabs) equilibrated with buffer AF. After loading, the column
295 was washed with 5 column volumes buffer AF, followed by buffer BF (50 mM Tris-
296 HCl, pH 7.4) until the baseline was stable. MBP-tagged SepF variants were eluted
297 with buffer BF containing 10 mM maltose. Appropriate fractions were pooled and
298 digested with factor Xa protease (New England Biolabs) in the presence of 2 mM
299 $CaCl_2$ at 4 °C overnight. *B. cereus* SepF was soluble while the others precipitated
300 after cleavage (*B. subtilis, S. pneumoniae, C. perfringens, M. tuberculosis,* all
301 chimera proteins) due to presence of calcium. Insoluble proteins were separated
302 from soluble MBP and factor Xa by centrifugation at 10,000 x g. Pellets containing
303 pure SepF were dissolved in buffer BF without $CaCl_2$, flash-frozen in liquid nitrogen
304 and stored at -80 °C until further use. SepF variants that were soluble after factor
305 Xa cleavage were separated from MBP and Factor Xa protease by ion exchange
306 chromatography. To this end, digested samples were loaded onto a 1 ml HiTrap Q
307 column (GE Healthcare) equilibrated with buffer BF. The column was washed with
308 buffer BF until the baseline was stable, followed by washing with 7.5% buffer CF
309 (50 mM Tris-HCl, pH 7.4, 1 M KCl) resulting in elution of MBP, and washing with
310 17.5% buffer CF resulting in elution of factor Xa. Pure SepF was eluted with 50%
311 buffer CF, flash-frozen in liquid nitrogen, and stored at -80 °C.

312

313 **Atomic force microscopy**

314 Purified *B. subtilis* SepF was diluted 1:10 in buffer BF and added onto a freshly
315 cleaved highly oriented pyrolytic graphite (HOPG) surface (Agar Scientific) and
316 allowed to settle for 20 min at room temperature prior to imaging in buffer solution
317 (36). Images were taken with an atomic force microscope from Nanotec
318 Electronica (Tres Cantos) operated in jumping mode at room temperature.
319 Olympus OMCL-RC800PSA rectangular, silicon-nitride cantilevers with a nominal
320 tip radius of 15 nm and a nominal spring constant of 0.05 N/m were used. Images
321 were processed and analyzed with WSxM software (37).

322

323 **Fluorescence light microscopy of liposomes**

324 Liposomes were prepared from *E. coli* polar lipid extract (Avanti Polar Lipids) as
325 described previously (6). Liposomes were extruded through 0.2 µm filters.
326 Samples were stained with 1 µg/ml Nile red, spotted on 1.2% agarose films,
327 covered with poly-dopamine-coated cover slips (38), and immediately imaged with
328 a Nikon Eclipse Ti equipped with a CFI Plan Apochromat DM 100x oil objective, an
329 Intensilight HG 130 W lamp, a C11440-22CU Hamamatsu ORCA camera, and NIS
330 elements software. Images were analyzed using ImageJ (National Institutes of
331 Health).

332

333 **Structured illumination (SIM) microscopy**

334 Liposomes for SIM were prepared from *E. coli* polar lipid extract (Avanti Polar
335 Lipids) as described previously (6). Liposomes were extruded through 0.8 µm
336 filters to obtain large enough vesicles. 0.25 mg/ml of the respective SepF variants
337 was mixed with 2 mg/ml liposomes in SepF binding buffer. Samples were stained

338 with 0.5 µg/ml mitotracker green, spotted on 1.2% agarose films, covered with
339 poly-dopamine-coated cover slips (38), and immediately imaged with a Nikon
340 Eclipse Ti N-SIM E microscope setup equipped with a CFI SR Apochromat TIRF
341 100x oil objective (NA1.49), a LU-N3-SIM laser unit, an Orca-Flash 4.0 sCMOS
342 camera (Hamamatsu Photonics K.K.), and NIS elements Ar software. SIM
343 microscopy of bacteria was performed by staining cells with 0.5 µg/ml mitotracker
344 green for 1 min, spotted on a thin film of 1.2% agarose (21).
345
346 **Transmission electron microscopy of proteins**
347 Protein samples were spotted on glow-discharged 200 mesh formvar/carbon-
348 coated copper grids (Agar Scientific) and incubated for 1 min at room temperature.
349 Excess liquid was removed with paper tissue and samples were negatively stained
350 by adding 100 µl 2% uranyl acetate drop by drop. Excess staining solution was
351 removed with paper tissue and samples were allowed to air dry. Samples were
352 examined with a JEOL1010 at 60 kV.
353
354 **Growth conditions for microscopy**
355 *B. cereus, S. pneumoniae*, and *C. perfringens* were grown on tryptic soy agar
356 plates containing 5 % sheep blood (BioMerieux). After three days of aerobic (*B.*
357 *cereus* and *S. pneumoniae*) or anaerobic incubation (*C. perfringens*) at 37 °C,
358 colonies were transferred to fresh plates and incubated for another 48 h prior to
359 suspension in phosphate-buffered saline and preparation for electron microscopy.
360 *B. subtilis* strains were grown in Luria-Bertani (LB) broth at 37 °C under steady
361 agitation. The medium was supplemented with 0.1 mM IPTG to induce expression
362 of SepF variants, where appropriate. It is important not to use more IPTG since
363 SepF overproduction causes membrane deformations that obscure septa (39).

364 Overnight cultures were grown with appropriate antibiotic concentrations (100
365 µg/ml spectinomycin, 10 µg/ml chloramphenicol, 5 µg/ml kanamycin, 1 µg/ml
366 erythromycin), where necessary. Cells were grown until exponential phase (OD_{600}
367 = 0.4) prior to microscopy.
368
369 **Transmission electron microscopy of bacteria**
370 Electron microscopy of bacteria was performed according to van Wezel *at al.*
371 (40)(*B. cereus*, *S. pneumoniae*, *C. perfringens)* or Saeloh *et al.* (41) (*B. subtilis*).
372 Samples were examined with a JEOL 1010 at an electron voltage of 60 kV.
373

Acknowledgements

We gratefully acknowledge Zehui Zhang and Daniel Antwi-berko for help with sample preparation, Wiep Klaas Smits for help with growing strains, Marien P. Dekker and Jan R. T. van Weering for support with TEM, and Gaurav Dugar for critically reading the manuscript. Electron microscopy was performed at the VU/VUMC EM facility, supported by the Netherlands Organization for Scientific Research (NWO, middelgroot 91111009). This work was financially supported by the Netherlands Organization for Scientific Research (NWO, STW-Vici 12128 to LWH and NWO-Vidi to WHR). MW was supported by a postdoc stipend from the Amsterdam Infection and Immunity Institute.

Conflict of Interest

The authors declare that this work was conducted in the absence of any commercial or financial relationships that could be construed as a potential conflict of interest.

Author contributions

MW planned and performed experiments and wrote the paper. INCG constructed strains and performed experiments. YG constructed strains. JW and MGM performed experiments. GJLW and WHR provided tools and planned experiments. LWH designed the study and wrote the paper.

395 **References**

396

397 1. Lutkenhaus J, Pichoff S, Du S (2012) Bacterial cytokinesis: From Z ring to
398 divisome. *Cytoskeleton* 69(10):778–790.
399 2. Gamba P, Veening JW, Saunders NJ, Hamoen LW, Daniel RA (2009) Two-
400 step assembly dynamics of the Bacillus subtilis divisome. *J Bacteriol*
401 191(13):4186–4194.
402 3. Errington J, Daniel RA, Scheffers D-J (2003) Cytokinesis in bacteria.
403 *Microbiol Mol Biol Rev* 67(1):52–65, table of contents.
404 4. Hamoen LW, Meile J-C, De Jong W, Noirot P, Errington J (2006) SepF, a
405 novel FtsZ-interacting protein required for a late step in cell division. *Mol*
406 *Microbiol* 59(3):989–999.
407 5. Duman R, et al. (2013) Structural and genetic analyses reveal the protein
408 SepF as a new membrane anchor for the Z ring. *Proc Natl Acad Sci U S A*
409 110(48):E4601-10.
410 6. Strahl H, Hamoen LW (2010) Membrane potential is important for bacterial
411 cell division. *Proc Natl Acad Sci U S A* 107(27):12281–12286.
412 7. Pichoff S, Lutkenhaus J (2005) Tethering the Z ring to the membrane
413 through a conserved membrane targeting sequence in FtsA. *Mol Microbiol*
414 55(6):1722–1734.
415 8. Gueiros-Filho FJ, Losick R (2002) A widely conserved bacterial cell division
416 protein that promotes assembly of the tubulin-like protein FtsZ. *Genes Dev*
417 16(19):2544–2556.
418 9. Levin PA, Kurtser IG, Grossman AD (1999) Identification and
419 characterization of a negative regulator of FtsZ ring formation in Bacillus
420 subtilis. *Proc Natl Acad Sci U S A* 96(17):9642–9647.

421 10. Taguchi A, et al. (2019) FtsW is a peptidoglycan polymerase that is
422 functional only in complex with its cognate penicillin-binding protein. *Nat*
423 *Microbiol* 4(4):587–594.
424 11. Daniel RA, Harry EJ, Errington J (2000) Role of penicillin-binding protein
425 PBP 2B in assembly and functioning of the division machinery of Bacillus
426 subtilis. *Mol Microbiol* 35(2):299–311.
427 12. Daniel RA, Noirot-Gros M-F, Noirot P, Errington J (2006) Multiple
428 interactions between the transmembrane division proteins of Bacillus
429 subtilis and the role of FtsL instability in divisome assembly. *J Bacteriol*
430 188(21):7396–7404.
431 13. Gündoğdu ME, et al. (2011) Large ring polymers align FtsZ polymers for
432 normal septum formation. *EMBO J* 30(3):617–626.
433 14. Kotiranta A, Lounatmaa K, Haapasalo M (2000) Epidemiology and
434 pathogenesis of Bacillus cereus infections. *Microbes Infect* 2(2):189–198.
435 15. Bottone EJ (2010) Bacillus cereus, a volatile human pathogen. *Clin*
436 *Microbiol Rev* 23(2):382–398.
437 16. Antonation KS, et al. (2016) Bacillus cereus Biovar Anthracis Causing
438 Anthrax in Sub-Saharan Africa—Chromosomal Monophyly and Broad
439 Geographic Distribution. *PLoS Negl Trop Dis* 10(9):e0004923.
440 17. Hoffmaster AR, et al. (2004) Identification of anthrax toxin genes in a
441 Bacillus cereus associated with an illness resembling inhalation anthrax.
442 *Proc Natl Acad Sci* 101(22):8449–8454.
443 18. Hoffmann C, et al. (2017) Persistent anthrax as a major driver of wildlife
444 mortality in a tropical rainforest. *Nature* 548:82.
445 19. Prinz WA, Hinshaw JE (2009) Membrane-bending proteins. *Crit Rev*
446 *Biochem Mol Biol* 44(5):278–291.

447 20. Velayati AA, Farnia P (2016) *Altas of Mycobacterium tuberculosis*
448 (Academic Press, Cambridge). 1st Editio.
449 21. Typas A, et al. (2010) Regulation of peptidoglycan synthesis by outer-
450 membrane proteins. *Cell* 143(7):1097–1109.
451 22. Krupka M, et al. (2017) Escherichia coli FtsA forms lipid-bound minirings
452 that antagonize lateral interactions between FtsZ protofilaments. *Nat*
453 *Commun* 8:15957.
454 23. Bisson-Filho AW, et al. (2017) Treadmilling by FtsZ filaments drives
455 peptidoglycan synthesis and bacterial cell division. *Science*
456 355(6326):739–743.
457 24. Krol E, et al. (2012) Bacillus subtilis SepF binds to the C-terminus of FtsZ.
458 *PLoS One* 7(8):e43293.
459 25. Buske PJ, Mittal A, Pappu R V, Levin PA (2015) An intrinsically disordered
460 linker plays a critical role in bacterial cell division. *Semin Cell Dev Biol*
461 37:3–10.
462 26. Jones LJ, Carballido-Lopez R, Errington J (2001) Control of cell shape in
463 bacteria: helical, actin-like filaments in Bacillus subtilis. *Cell* 104(6):913–
464 922.
465 27. Hussain S, et al. (2018) MreB filaments align along greatest principal
466 membrane curvature to orient cell wall synthesis. *Elife* 7:e32471.
467 28. Ursell TS, et al. (2014) Rod-like bacterial shape is maintained by feedback
468 between cell curvature and cytoskeletal localization. *Proc Natl Acad Sci U S*
469 *A* 111(11):E1025-34.
470 29. Dominguez-Escobar J, et al. (2011) Processive movement of MreB-
471 associated cell wall biosynthetic complexes in bacteria. *Science*
472 333(6039):225–228.

473 30. Garner EC, et al. (2011) Coupled, circumferential motions of the cell wall
474 synthesis machinery and MreB filaments in B. subtilis. *Science*
475 333(6039):222–225.
476 31. Riggs P (2001) Expression and Purification of Maltose-Binding Protein
477 Fusions. *Current Protocols in Molecular Biology* (John Wiley & Sons, Inc.).
478 doi:10.1002/0471142727.mb1606s28.
479 32. Yoshimura M, Oshima T, Ogasawara N (2007) Involvement of the
480 YneS/YgiH and PlsX proteins in phospholipid biosynthesis in both Bacillus
481 subtilis and Escherichia coli. *BMC Microbiol* 7(1):69.
482 33. Gibson DG, et al. (2009) Enzymatic assembly of DNA molecules up to
483 several hundred kilobases. *Nat Meth* 6(5):343–345.
484 34. Hauser PM, Karamata D (1994) A rapid and simple method for Bacillus
485 subtilis transformation on solid media. *Microbiology* 140(7):1613–1617.
486 35. Ishikawa S, Kawai Y, Hiramatsu K, Kuwano M, Ogasawara N (2006) A new
487 FtsZ-interacting protein, YlmF, complements the activity of FtsA during
488 progression of cell division in Bacillus subtilis. *Mol Microbiol* 60(6):1364–
489 1380.
490 36. Heinze K, et al. (2016) Protein Nanocontainers from Nonviral Origin:
491 Testing the Mechanics of Artificial and Natural Protein Cages by AFM. *J Phys*
492 *Chem B* 120(26):5945–5952.
493 37. Horcas I, et al. (2007) WSXM: A software for scanning probe microscopy
494 and a tool for nanotechnology. *Rev Sci Instrum* 78(1):13705.
495 38. te Winkel JD, Gray DA, Seistrup KH, Hamoen LW, Strahl H (2016) Analysis
496 of antimicrobial-triggered membrane depolarisation using voltage sensitive
497 dyes. *Front Cell Dev Biol* 4:29.
498 39. Gao Y, Wenzel M, Jonker MJ, Hamoen LW (2017) Free SepF interferes with

499 recruitment of late cell division proteins. *Sci Rep* 7(1):16928.
500 40. van Wezel GP, et al. (2000) ssgA is essential for sporulation of
501 Streptomyces coelicolor A3(2) and affects hyphal development by
502 stimulating septum formation. *J Bacteriol* 182(20):5653–5662.
503 41. Saeloh D, et al. (2018) The novel antibiotic rhodomyrtone traps membrane
504 proteins in vesicles with increased fluidity. *PLoS Pathog* 14(2):e1006876.
505

506 **Figure legends**

507

508 **Fig. 1** SepF forms rings and tubules. **(A)** Plane AFM images of three different SepF
509 rings imaged in buffer solution. **(B)** 3D projections of the same images. **(C)** Height
510 measurements of the individual SepF rings shown in A and B. **(D)** Height
511 measurements of SepF rings derived from AFM data. **(E)** TEM image of SepF stack
512 and tubules after cleavage from MBP. **(F)** TEM image of SepF rings after ion-
513 exchange chromatography. Scale bars 100 nm.

514

515 **Fig. 2** Membrane binding, ring formation and septum thickness. **(A)** Sequence
516 alignment (Clustal Omega) of SepF homologues used in this study. Dark and light
517 grey marks identical and similar amino acids, respectively. Arrows mark the
518 beginning and end of the highly conserved core domain. **(B)** Fluorescence light
519 microscopy image showing the aggregation of small liposomes (~200 nm) by
520 purified *S. pneumoniae* SepF. Liposomes were stained with Nile red. **(C)** SIM image
521 showing deformation of large liposomes (800 nm) by purified *S. pneumoniae* SepF.
522 Liposomes were stained with mitotracker green. 0.25 µg/ml SepF was mixed with
523 2 mg/ml liposomes. Scale bars 1 µm. See Fig. S3 for the results with other SepF
524 variants. **(D)** TEM pictures of purified SepF from the different species. Scale bar
525 50 nm. **(E)** Quantification of the inner SepF ring diameter. Black bars show mean
526 with standard error of the mean. A minimum of 45 rings was measured. **(F)** TEM
527 images of nascent cell division septa of the respective species. **(G)** Quantification
528 of the thickness of the nascent septa of the respective organisms. Black bars show
529 mean with standard error of the mean. A minimum of 50 septa was measured.
530 **(H)** Comparison of inner ring diameters with nascent septum thickness. Average
531 +/- standard deviations is indicated. *Data for *M. tuberculosis* were taken from

532 the literature (20). **(I)** Correlation between inner SepF ring diameter and septum
533 thickness (R^2=0.74).
534
535 **Fig. 3** The conserved core domain of SepF determines ring diameter. **(A)** TEM
536 pictures of purified SepF chimera proteins. **(B)** Quantification of ring diameter.
537 Black bars represent mean with standard error of the mean. A minimum of 50
538 rings was measured. **(C)** Comparison of the inner ring diameters of the original
539 and chimera proteins. Average +/- standard deviation is given. **(D)** Correlation
540 between original and chimera ring diameter (R^2=0.71).
541
542 **Fig. 4** SepF ring diameter determines septum thickness. **(A)** SIM images of *B.*
543 *subtilis* Δ*sepF* cells expressing different SepF chimera. The chimera were
544 expressed from the IPTG-inducible *Pspac* promotor. Cells were grown in the
545 presence of 100 µM IPTG until mid-log phase prior to membrane staining and
546 microscopy. Lack of SepF results in severely deformed septa, which shows as
547 highly fluorescent membrane patches due to membrane invaginations and double
548 membranes. Scale bar 2 µm. **(B)** Representative TEM images of septa of Δ*sepF*
549 strains expressing the different SepF chimeras. Scale bar 1 µm. **(C)** Quantification
550 of the septum thickness of the different strains. Black bars represent mean with
551 standard error of the mean. p values for *C. perfringens* and *M. tuberculosis*
552 chimeras compared to *B. subtilis* are <0.0001. **(D)** Comparison and **(E)** correlation
553 of the inner ring diameter of SepF chimeras and nascent septum thickness of *B.*
554 *subtilis* Δ*sepF* expressing the chimeras (R^2=0.57).
555
556 **Fig. 5** Clamp model illustrating how SepF polymers can control septal thickness.
557 SepF forms large rings with an average inner ring diameter (d) that corresponds

558 to the thickness of septa (t). Crossections of a nascent septum (grey) is depicted.
559 FtsZ polymers (Z) bind to the outside of SepF rings, in a perpendicular fasion. The
560 transmembrane peptidoglycan synthesis machinery (P) is associated with FtsZ
561 polymers. Of note, it is not yet know how these transmembrane proteins are linked
562 to FtsZ polymers in Gram-positive bacteria, and this association might be indirect.

563 **Fig. 1.**

564

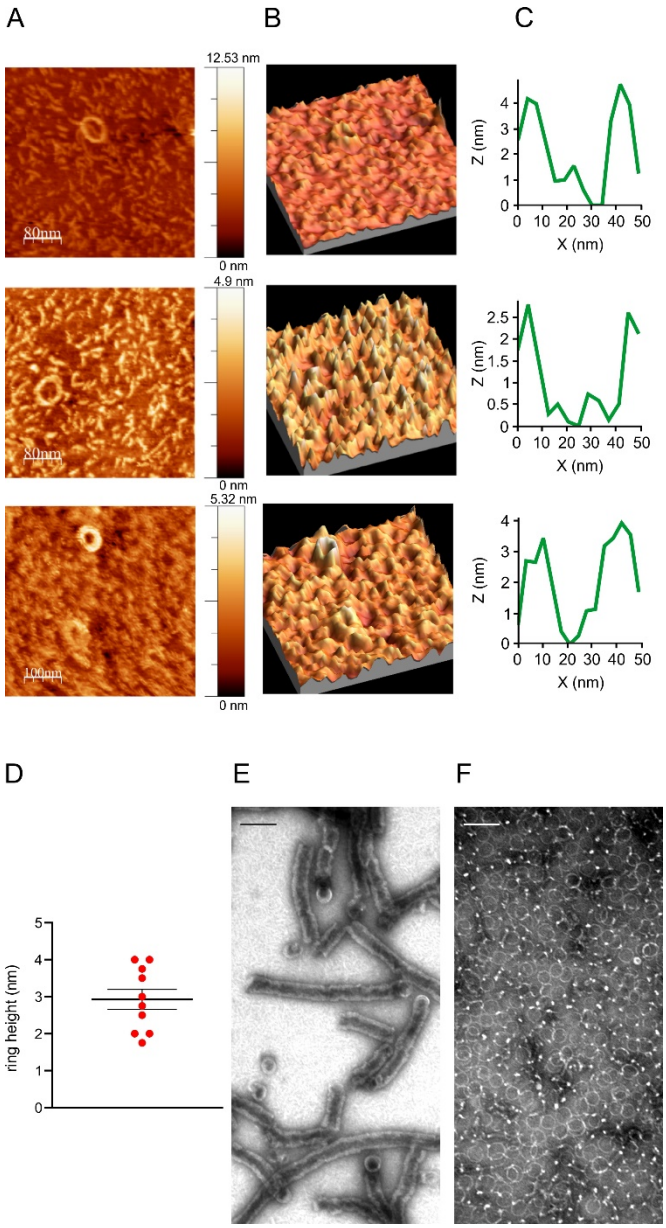
A
B
C
12.53 nm
0 nm
80nm
4.9 nm
0 nm
80nm
5.32 nm
0 nm
100nm
Z (nm)
X (nm)
D
E
F
ring height (nm)

565 **Fig. 2.**

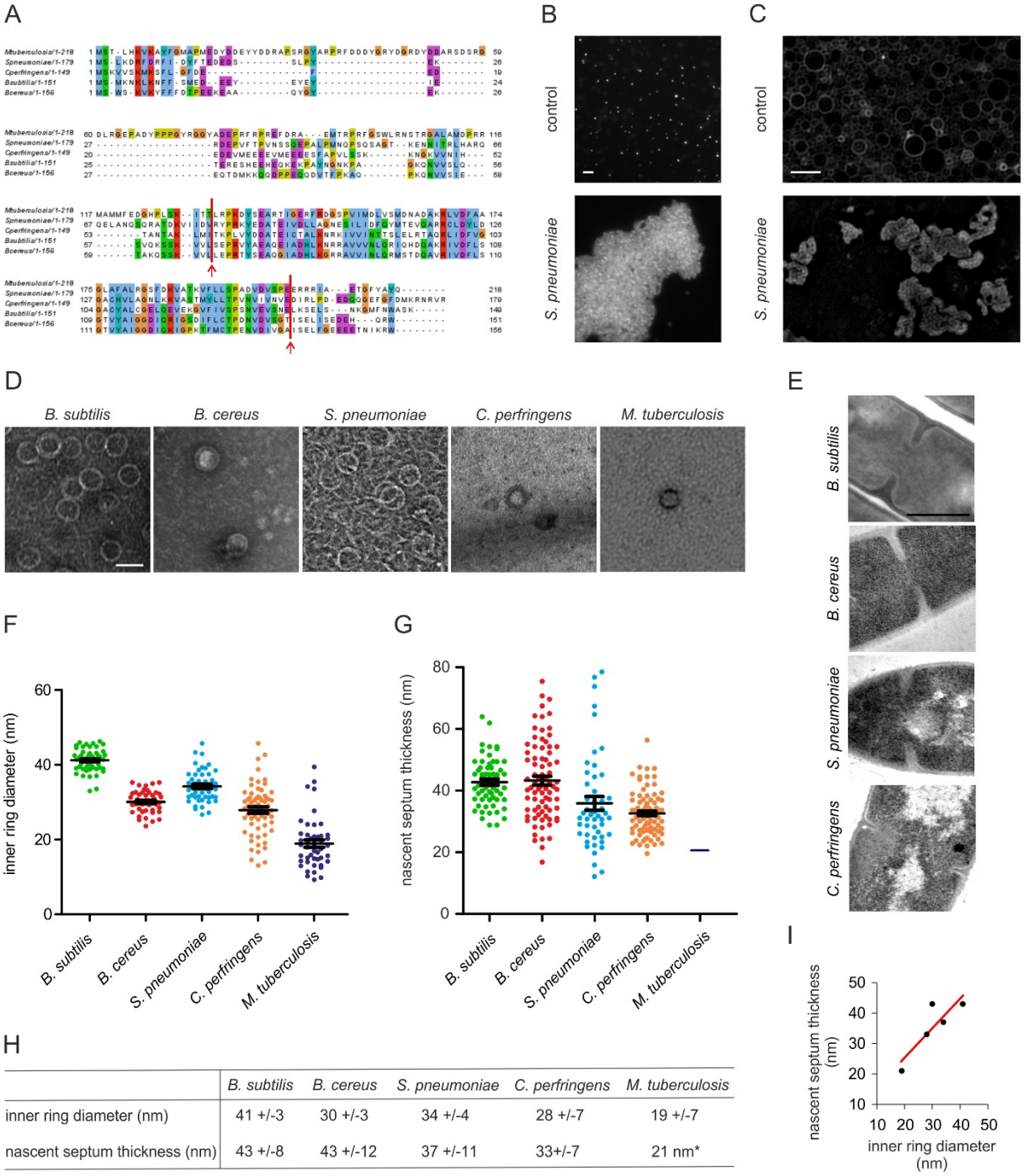

H

	B. subtilis	*B. cereus*	*S. pneumoniae*	*C. perfringens*	*M. tuberculosis*
inner ring diameter (nm)	41 +/-3	30 +/-3	34 +/-4	28 +/-7	19 +/-7
nascent septum thickness (nm)	43 +/-8	43 +/-12	37 +/-11	33+/-7	21 nm*

566 **Fig. 3.**

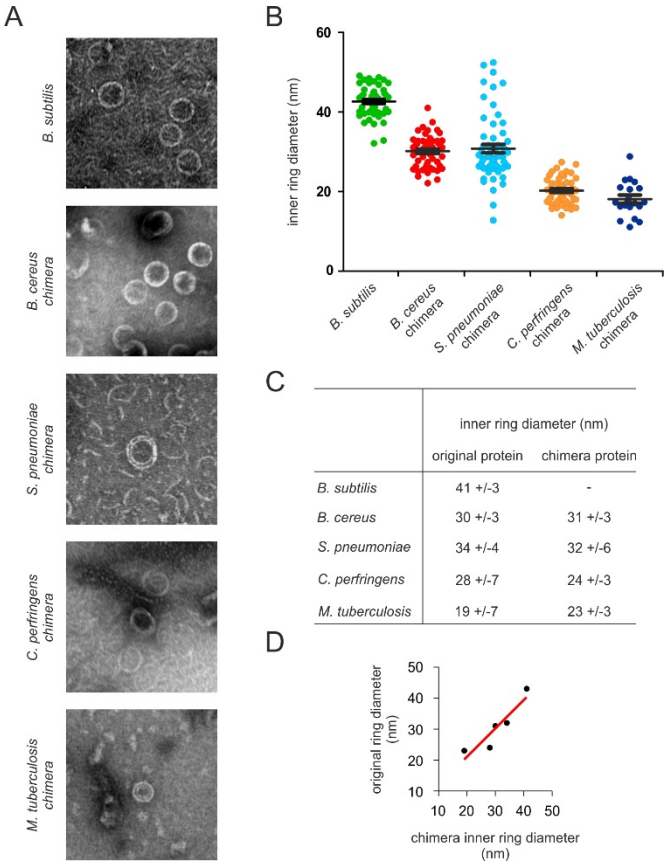

	inner ring diameter (nm)	
	original protein	chimera protein
B. subtilis	41 +/-3	-
B. cereus	30 +/-3	31 +/-3
S. pneumoniae	34 +/-4	32 +/-6
C. perfringens	28 +/-7	24 +/-3
M. tuberculosis	19 +/-7	23 +/-3

567 **Fig. 4.**

568

A

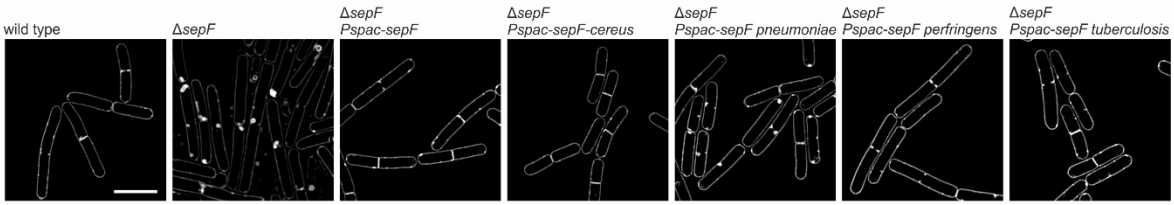

B

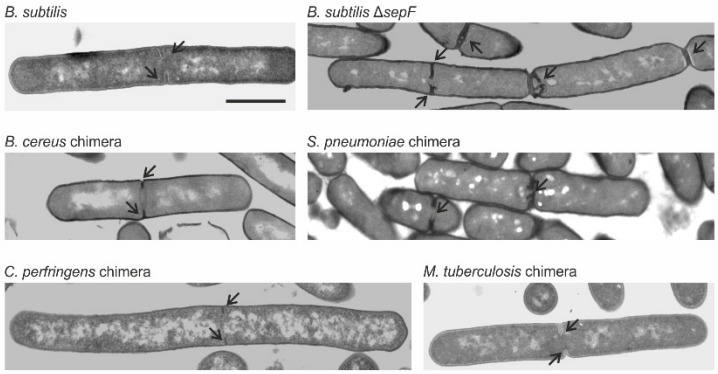

C

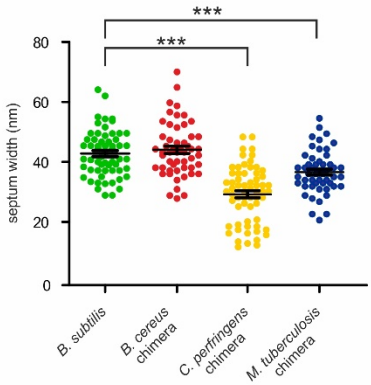

D

	B. subtilis	*B. cereus*	*C. perfringens*	*M. tuberculosis*
inner ring diameter chimeras (nm)	41 +/-3	31 +/-3	24 +/-3	23 +/-3
nascent septum thickness chimeras (nm)	43 +/-8	44 +/-9	28 +/-7	35 +/-10

E

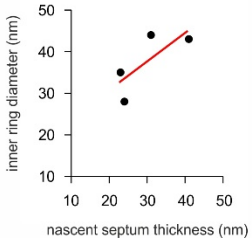
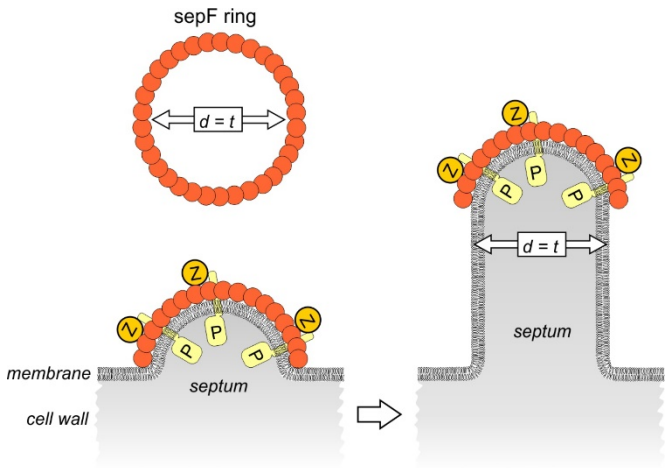
569 **Fig. 5.**